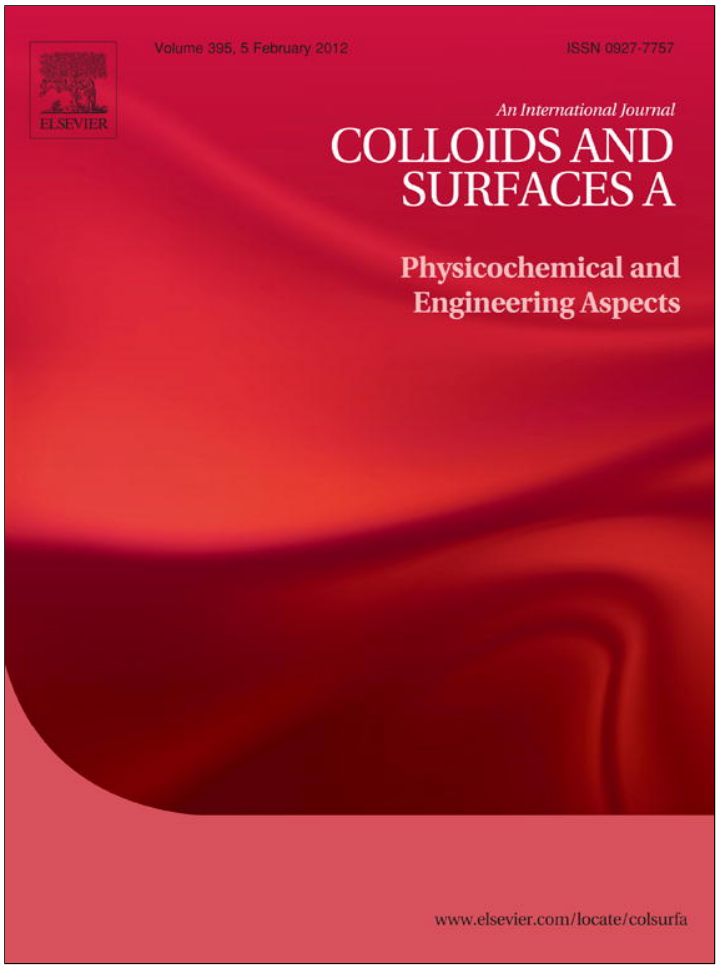

Colloids and Surfaces A: Physicochem. Eng. Aspects 395 (2012) 10–17

Contents lists available at SciVerse ScienceDirect

Colloids and Surfaces A: Physicochemical and Engineering Aspects

journal homepage: www.elsevier.com/locate/colsurfa

Surfactant-assisted formation of organophilic CeO_2 nanoparticles

Özge Tunusoğlu[a], Rafael Muñoz-Espí[c], Ümit Akbey[d], Mustafa M. Demir[a,b,*]

[a] Izmir Institute of Technology, Department of Chemistry, 35430 Gulbahce, Urla, Izmir, Turkey
[b] Izmir Institute of Technology, Materials Science and Engineering Program, 35430 Gulbahce, Urla, Izmir, Turkey
[c] Max Planck Institute for Polymer Research, Ackermannweg 10, 55128 Mainz, Germany
[d] FMP Leibniz-Institut für Molekulare Pharmakologie, NMR Supported Structural Biology, Robert-Roessle-Str. 10, 13125 Berlin, Germany

ARTICLE INFO

Article history:
Received 3 September 2011
Received in revised form
17 November 2011
Accepted 18 November 2011
Available online 16 December 2011

Keywords:
Ceria
Controlled precipitation
Rare-earth metal oxide
Surface modification
Redispersible nanoparticles

ABSTRACT

We report a simple one-pot method to prepare organically functionalized CeO_2 nanoparticles by controlled chemical precipitation. The particles were nucleated by mixing aqueous solutions of $Ce(NO_3)_3{\cdot}6H_2O$ and ammonia at room temperature. Different small organic molecules were chosen as capping agents and injected into the reaction medium at the beginning of the synthesis: 3-(mercaptopropyl) trimethoxy silane (MPS), hexadecyltrimethyl ammonium bromide (CTAB), 3-mercapto propionic acid (3-MPA), and thioglycolic acid (TGA). The resulting nanocrystals were quasi-spherical and had a narrow mean size distribution with an average size smaller than 10 nm. Dynamic nuclear polarization enhanced NMR (DNP-NMR) and FTIR measurements suggested a chemical grafting of the surfactant and a homogeneous surface modification. The colloidal stabilities were characterized by dynamic light scattering and zeta potential measurements. The stabilization by aliphatic groups was tested with a frequently used hydrophobic monomer, methyl methacrylate. According to the results, CTAB is the most effective of the used stabilizing surfactant. The mechanism of formation of the organophilic CeO_2 nanoparticles is discussed.

1. Introduction

Rare-earth metal oxides arise great interest in materials science, because the presence of 4f electrons results in attractive optical, magnetic, and chemical properties [1]. Ceria (CeO_2) is one of the most frequently studied rare earth metal oxides and possesses unique physicochemical properties, such as absorption of ultraviolet radiation [2], gas sensing [3], and catalytic properties [4,5]. Moreover, it is a wide band gap semiconductor, with a band gap of 3.2 eV [6]. Most of the advanced applications of CeO_2 generally appear in the nanosized regime, in which many physical properties are strongly size dependent and show significant quantum size effects. Many new potential applications for nanometric ceria—including solar cells, nanolasers, and other highly functional and effective devices—are under current discussion [7]. The synthesis of nanosized ceria particles have been achieved by many different methods. Supercritical hydrothermal [1], conventional hydrothermal [8], solvothermal [9], and pyrolytic [10] syntheses are the four major methods to fabricate nanosized powder. The synthesis methods require hard conditions at extreme temperature and pressure; they are also still limited in the amount of nanoparticles. However, chemical precipitation provides a promising pathway for large scale production of nanosized particles at ambient conditions [11–13].

Polymer/nanoparticle composites with tunable composition and morphology often exhibit multiple functionalities and even novel properties [14], which may lead to applications in diverse areas such as optoelectronics. The performance of composite materials strongly depends on the homogeneity of the particle dispersion. The control of the surface chemistry of particles is a key point to obtain well-defined and homogeneous dispersions of host particles in guest polymer matrices. Post-synthetic modification has usually been employed to introduce desired functionalities onto the surface of nanoparticles. Nanoparticles are typically treated with surfactant molecules in dispersion. This treatment modifies the surface chemistry of particle domains, which are generally formed by pseudo-aggregates of a group of particles. Thus, the surface cannot be functionalized evenly and the particle dispersion is negatively affected. The precipitation in the presence of surfactant molecules (i.e., controlled precipitation) is an efficient approach to obtain homogeneous surface modification of the particles in one step and it allows the size and the surface chemistry to be controlled [15].

The use of a minute amount of a surface-active reagent—which could be a small molecule or a macromolecule—in the reaction mixture has been considered a powerful pathway to prepare

* Corresponding author at: Izmir Institute of Technology, Department of Chemistry, 35430 Gulbahce, Urla, Izmir, Turkey. Tel.: +90 232 750 75 11; fax: +90 232 750 75 09.
E-mail address: mdemir@iyte.edu.tr (M.M. Demir).

0927-7757/$ – see front matter © 2011 Elsevier B.V. All rights reserved.
doi:10.1016/j.colsurfa.2011.11.026

nanoparticles with a desired surface chemistry [16,17]. Recently, Taniguchi et al. reported the synthesis of organophilic CeO_2 nanoparticles by a single step reaction of a cerium oleate complex with NH_4OH [18]. The reaction was carried out at room temperature in an aqueous medium. The authors claimed that the oleate links to the surface of CeO_2 particles by chemical bonding and render the particles surface an organophilic nature. The same research group performed supercritical hydrothermal synthesis of hydrophilic polymer-modified CeO_2 nanoparticles. Water-soluble polymers (e.g., polyvinyl alcohol or polyacrylic acid) were employed in the reaction mixture as surface modifiers. As a result, 20 nm cuboctahedral water-dispersible CeO_2 nanoparticles were obtained [19]. Using a similar strategy, Yu et al. synthesized high quality CeO_2 nanocrystals by stabilization with the double hydrophilic block copolymer poly(ethylene glycol)-*block*-poly(methacrylic acid) as a stabilizer [20]. Monodisperse CeO_2 particles with less than 2 nm diameter were synthesized by hydrothermal hydrolysis at 120 °C.

In the present work, we report a novel and very versatile synthesis of surface-functionalized CeO_2 nanocrystals by chemical precipitation at room temperature in aqueous solutions containing various capping agents. Nanoparticles with a variety of surface chemistry can be prepared. Four small surfactant molecules were used: 3-(mercaptopropyl) trimethoxy silane (MPS), hexadecyltrimethyl ammonium bromide (CTAB), 3-mercapto propionic acid (3-MPA), and thioglycolic acid (TGA). The dispersibility of the produced particle domains were investigated in a hydrophobic monomer, methyl methacrylate, by determining the particle size distribution by DLS.

2. Experimental

2.1. Synthesis of CeO_2 nanoparticles

Colloidal cerium(IV) oxide particles were synthesized at 22 °C, by reacting 10 mL of an aqueous solution of $Ce(NO_3)_3{\cdot}6H_2O$ (0.05 M, Merck, extra pure solution) and 10 mL of ammonia (0.5 M, Merck) for 3 h. The precipitation was repeated in the presence of various surfactants: 3-(mercaptopropyl) trimethoxy silane (MPS, Aldrich, 95%), hexadecyltrimethyl ammonium bromide (CTAB, Aldrich), 3-mercapto propionic acid (3-MPA, Alfa Aesar), and thioglycolic acid (TGA, Merck). 2.65×10^{-5} mol of each surfactant was added to the mixture at the first minute of reaction. The nanoparticles obtained were separated from the solution mixture by centrifugation at 6000 rpm for 1 h. After washing twice with deionized water and ethanol, the product was dried overnight in a vacuum oven at 45 °C. All reagents were used without further purification.

2.2. Characterization

Transmission electron microscopy (TEM) was carried out in a Zeiss EM 902 microscope operated at 80 kV. High-resolution TEM micrographs were obtained with a FEI Technai F20 microscope operated at 200 kV. The phase structure of synthesized particles were characterized by X-ray diffraction (XRD, Philips X'pert Pro) with a Cu Kα radiation source (λ = 1.54 Å). The average size of crystallites was determined by Scherrer's equation

$$t = \frac{0.9\lambda}{B \cos\theta} \quad (1)$$

where t is the diameter of the particle, λ is the wavelength of Cu Kα radiation (1.542 Å) and B is the line broadening (full width at half maximum), θ is the angle of the peak center. Fourier transform infrared (FTIR) spectra were registered by using a Perkin Elmer Spectrum 100 instrument (4000–400 cm^{-1}, 20 scans, resolution of 4 cm^{-1}). Thermogravimetric analysis was performed under nitrogen in a Mettler Toledo ThermoSTAR TGA/SDTA 851 thermobalance by heating from room temperature to 1000 °C at a heating rate of 10 °C min^{-1}. The size distributions of particles dispersed in methyl methacrylate (Fluka) were investigated by dynamic light scattering (DLS, Malvern Zetasizer Nano-ZS Nano Series). The viscosity and refractive index of the medium were specified as 0.584 mPa s and 1.414 (20 °C), respectively. Photoluminescence emission spectra of dispersions in methyl methacrylate were determined in a Varian Cary Eclipse Fluorescence spectrophotometer by exciting at 250 nm and observing the emission between 300 and 450 nm. ^{13}C cross-polarization (CP) magic-angle spinning (MAS) nuclear magnetic resonance (NMR) spectra were recorded in a Bruker Avance spectrometer at 100.6 MHz ^{13}C Larmor frequency. All CP-MAS spectra have been recorded with 1 s recycle delay, 2 ms CP contact time, 100 kHz RF nutation frequency for proton and carbon (2.5 μs for 90° pulse length), at ~9 kHz MAS frequency, and by using the TPPM scheme for proton decoupling. 50 and ~59 kHz spin lock pulses were used for the cross-polarization transfer.

3. Results and discussion

3.1. Structural and morphological characterization of CeO_2 nanoparticles

Crystalline CeO_2 nanoparticles were precipitated by mixing aqueous solutions of cerium nitrate and ammonia at room temperature. Four molecules with different structures and functionalities, shown in Scheme 1, were used as capping agents.

It is known that ceria, of cubic fluorite structure, develops from either spherical [21] or rod-like [22] morphology to truncated

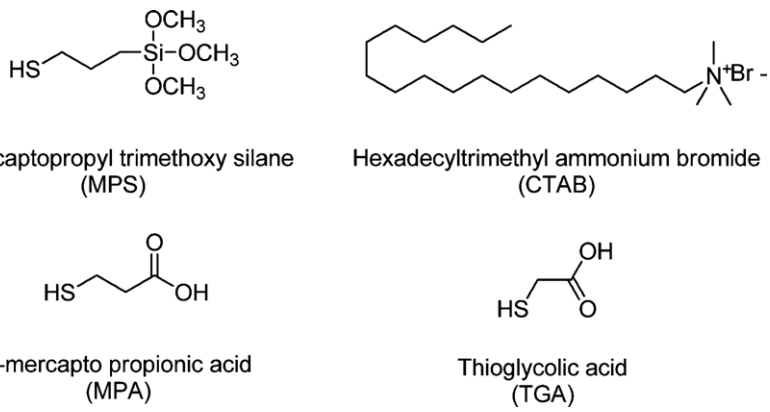

3-mercaptopropyl trimethoxy silane (MPS)

Hexadecyltrimethyl ammonium bromide (CTAB)

3-mercapto propionic acid (MPA)

Thioglycolic acid (TGA)

Scheme 1. Chemical structures of the surfactants.

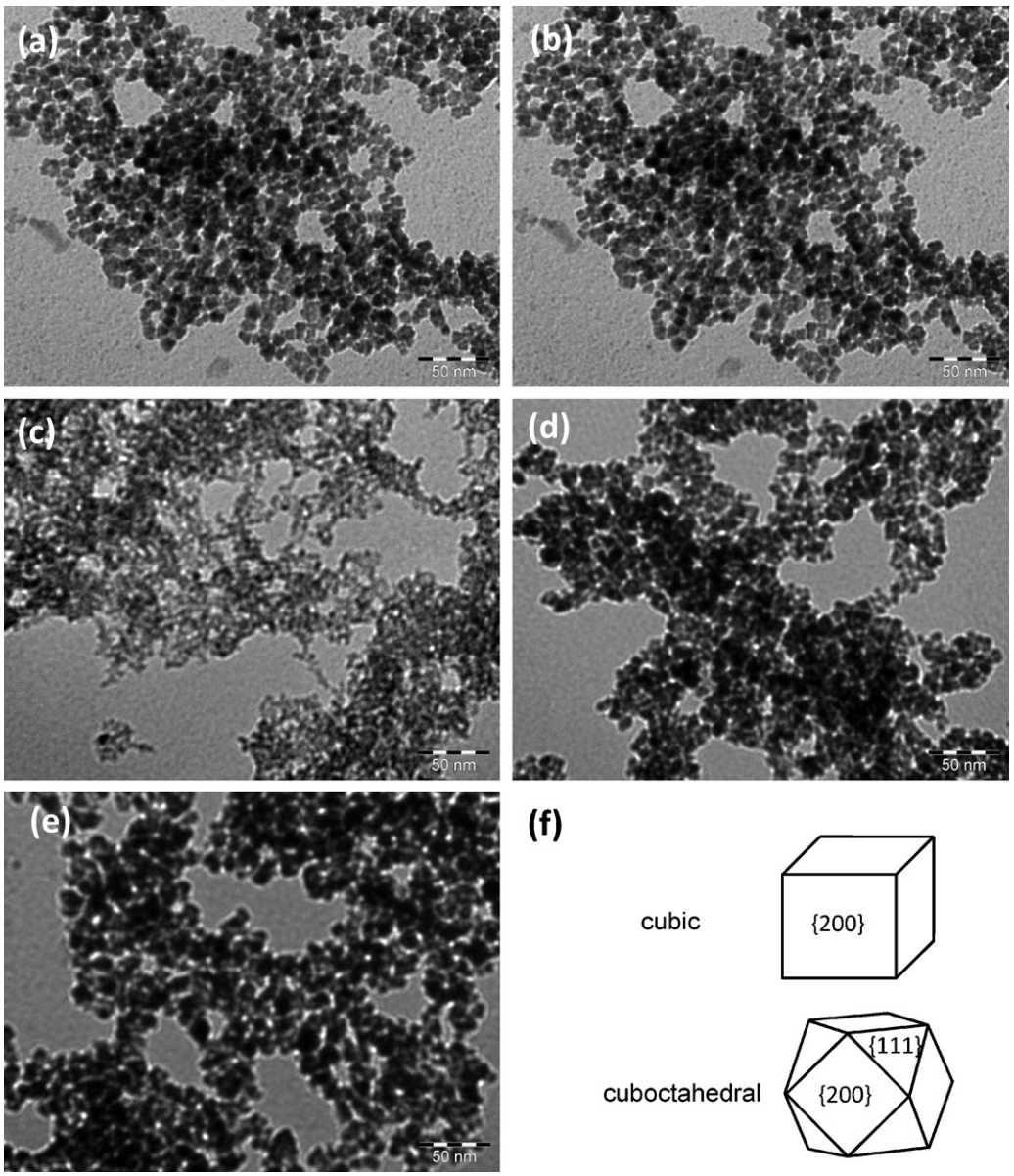

Fig. 1. TEM micrographs of CeO_2 particles synthesized with NH_3: (a) unmodified; and modified by (b) CTAB, (c) MPS, (d) 3MPA, (e) TGA, and (f) structural models of the cubic and octahedra.

octahedral, which gradually convert to a cubic shape, independently of the initial morphology. Fig. 1 contains overview TEM micrographs of both unmodified and modified CeO_2 nanoparticles, as well as structural models of the cubic and cuboctahedral crystals. An average size of about 5 nm was estimated for the functionalized nanoparticles by measuring the size of more than 50 particles in the TEM micrographs.

High resolution TEM micrographs provided more detailed information about the morphology of our nanoparticles. Capturing images of individual unmodified particles is a hard task because the unmodified particles have, in general, strong tendency to aggregate to reduce the surface area/volume ratio. Nevertheless, individual particles in the aggregates showed a cuboctahedral shape, as seen in the representative example indicated by an arrow in Fig. 2a. The micrographs of Fig. 2b–c shows that the particles precipitated in the presence of CTAB and MPS have a cubic morphology. Each particle is a well-ordered single crystal with a fringe distance of 0.31 nm corresponding to the (1 1 1) lattice plane of ceria. Furthermore, lattice fringes for (2 2 0) and (2 0 0) are evident.

The yield of the precipitation reaction, presented in the second column of Table 1, lies between 50 and 70%.

Fig. 3 shows X-ray diffraction (XRD) patterns of the CeO_2 nanoparticles. Reflections for all samples agree well with those of cubic ceria CeO_2 (JCPDS Card No. 81-0792), whose patterns are given as vertical drop lines at the bottom of the diffractograms.

Table 1
Crystal size values of the synthesized ceria nanoparticles under ambient pressure and at room temperature. The size of crystals was obtained from XRD pattern by using Scherrer's equation taking into account (1 1 1) reflection. Yield was obtained gravimetrically.

Sample	Yield (%)	D_{TEM} (nm)	D_{XRD} (nm)
CeO_2	50	5 ± 2	8
CeO_2-MPS	70	4 ± 2	4
CeO_2-CTAB	60	6 ± 1	10
CeO_2-3MPA	49	4 ± 1	6
CeO_2-TGA	58	5 ± 3	6

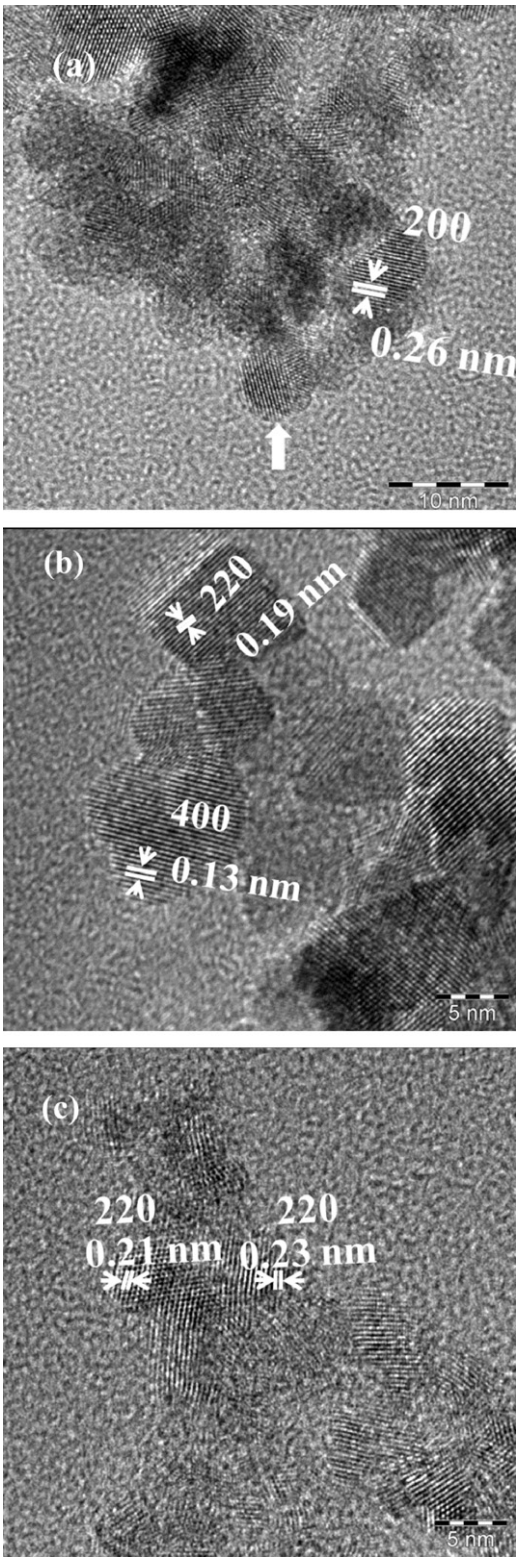

Fig. 2. High resolution TEM micrographs of CeO_2 particles (a) unmodified and modified by (b) CTAB and (c) MPS.

The crystallite sizes, given in the fourth column of Table 1, were calculated by Scherrer's equation.

3.2. Surface chemistry and stability of particle dispersion

The control of the surface chemistry is important not only for the compatibility of the particles with organic media but also for reaching certain properties such as roughness, hydrophobicity, surface charge, surface energy, and reactivity. Both Fourier transform infrared (FTIR) spectroscopy and nuclear magnetic resonance (NMR) were used to examine the functional groups present on the surface of the CeO_2 nanoparticles. FTIR spectra for unmodified and CeO_2 nanoparticles modified with different surfactants are presented in Fig. 4.

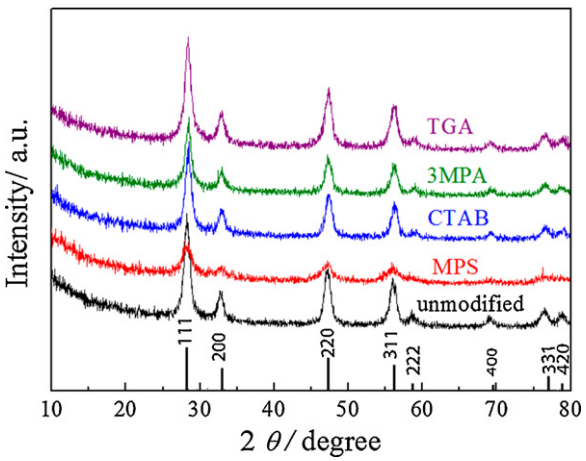

Fig. 3. XRD patterns of the as-synthesized CeO_2 particles.

Two signals are commonly observed in all spectra: (i) the broad band centered around 3300–3400 cm^{-1}, which is attributed to OH stretching; and (ii) a narrow peak at 1384 cm^{-1}, originating from nitrate groups. The spectra of the surface-modified particles were compared with that of the corresponding pure surfactant. As each surfactant has its own characteristic signals, the grafting of surfactant molecules on the particle surface could be determined from the appearance/disappearance of these signals. For example, for TGA and MPA, the SH band at 2800–2500 cm^{-1} disappears while the bands of the —OCH_3 group remains at 1676 cm^{-1}. A condensation takes place between —SH and surface —OH groups, leading to a grafting of the molecules to the particle surface. Similarly, when using MPS as a surfactant, a new band attributed to the Si—O—C bond appears (Fig. 4). For CTAB-capped particles, the vibrations of CH_2 bending are remarkably enhanced after modification.

Compared to the significantly much larger mass/volume of the bulk CeO_2 nano-particles, the surface surfactants sites represent a relatively very small percentage of the whole studied material. As a result, conventional NMR techniques have difficulties to observe such surface species with small quantities. Dynamic

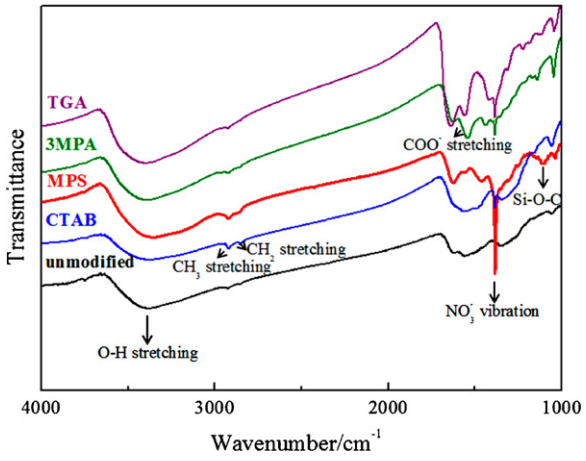

Fig. 4. FTIR spectra of the as-synthesized CeO_2 particles.

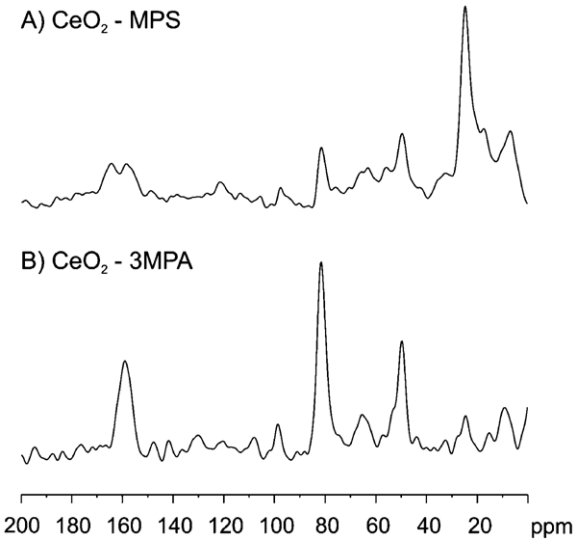

Fig. 5. CP-MAS spectrum of the surface modified CeO_2 materials in the presence of MPS, and 3MPA.

nuclear polarization (DNP), a recently introduced technique, has been proven to be very successful in increasing the sensitivity of the NMR signal several orders of magnitude for both synthetic functional and bio materials [23–26]. Although the DNP method is well established when applied to the biological materials, very few examples about its application to synthetic materials have been demonstrated at high magnetic fields up to now [24,26,27]. Especially, the need to mix the electron source, a radical which is mostly 1-(2,2,6,6-tetramethyl-1-oxy-4-piperidinyl)oxy-3-(2,2,6,6-tetramethyl-1-oxy-4-piperidinyl)amino-propan-2-ol (TOTAPOL), with insoluble materials is one of the big challenges of this very promising technique.

Here, we present the utilization of ^{13}C CP-MAS NMR spectroscopy performed at low temperatures (~100 K) for the proof-of-principle demonstration on two selected examples of the synthesized nano-materials, MPS and 3MPA modified CeO_2 nano-materials. This method is a first step to the final DNP characterization of the surface species of these nano-materials, and for the moment only ensures the utilization of the larger Boltzman polarization as a result of lower temperatures to increase the sensitivity of the NMR experiment. The detailed study on the DNP enhanced NMR spectroscopy with the use of radical is in progress in our group. The ^{13}C CP-MAS spectra were recorded for the CeO_2 nanoparticles functionalized with MPS and 3MPA-materials are represented in Fig. 5. The spectra were recorded at ~100 K, ~9 kHz MAS and in ~12 h each. The spectra show clear signals from the surface surfactant species (from CH_2, OCH_3, and carboxylic carbon sites), and proves the successful modification of the surface of the nanomaterial with MPS and 3MPA. With the detection of trace-amount of functional surface species, significant changes in the surface composition of the nanoparticles were determined, as seen in Fig. 5.

Although the product has the same physical features in bulk, the preparation method and starting materials can give rise to different nucleation and growth behaviors, which may result in the formation of defects in the crystal structure. Defects have a strong impact on electronic transitions and, thus, on the optical properties. Fig. 6 shows that room-temperature photoluminescence (PL) emission spectra of samples prepared in the presence of the surfactants are very similar to that of the unmodified sample, demonstrating that the presence of surfactants does not significantly affect the optical properties.

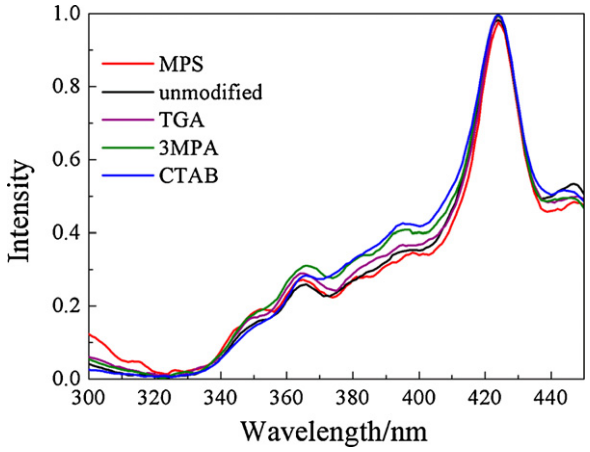

Fig. 6. Fluorescence spectra of the as-synthesized CeO_2 particles.

Both unmodified and modified CeO_2 particles showed a strong PL emission signal at 424 nm, a faint shoulder around 395 nm, and two broad emissions centered at 365 nm and 350 nm. The spectra are normalized with respect to the most intense signal at 424 nm to examine the effect of surfactants on the emission. The emission bands at 424 nm and 394 nm are generally attributed to charge transfer from O_2 to Ce^{4+}, that is, electron transition or charge transfer from oxygen vacancies [5,28,29]. The two weak and broad signals at 365 nm and 350 nm are ascribed to charge transfer transition from O^{2-} to Ce^{4+} [12,30].

Thermal degradation of synthesized cerium oxide nanoparticles was studied by thermogravimetric analysis under nitrogen flow. Fig. 7 shows thermograms of unmodified and surface-modified cerium oxide nanoparticles.

A continuous mass loss is observed until ca. 800 °C for all samples. After that temperature, the curves reach a plateau that corresponds to ca. 93% loss for the unmodified sample and to 85–92% for the surfactant-modified samples. From the difference between the mass loss between the unmodified and the modified samples, the content of organic component in the samples was estimated to range between 0.6 wt% (for 3MPA) and 7.8 wt% (for MPS). The results suggest that a crystalline core of CeO_2 particles is covered with a thin layer of organic groups. Using the estimated individual particle size from TEM micrographs and assuming that the density of CeO_2 nanoparticles is equal to bulk density of CeO_2, one can estimate the number of surfactant molecules grafted to the surface of the particles. The third column of Table 2 presents the results of this estimation.

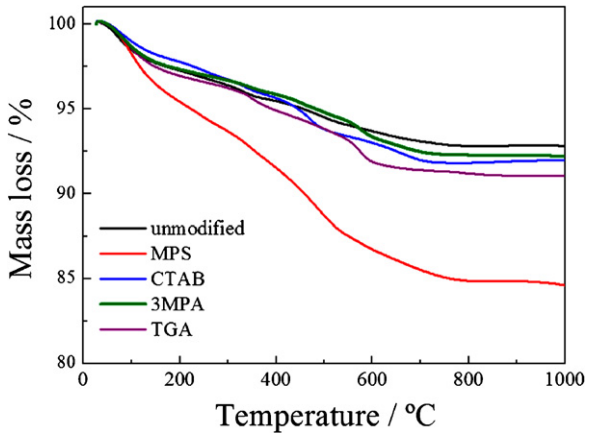

Fig. 7. Mass loss curves of the as-synthesized CeO_2 particles.

Table 2
Percent mass loss from the CeO_2 nanoparticles and surface coverage by modifier precipitated in the presence of various surfactants.

Modifier	Mass loss (%) from TGA	Coverage modifier (molecules/nm^2)
No modifier	7.3	–
MPS	15.1	2.5
CTAB	8.4	0.9
3MPA	7.9	2.4
TGA	9.0	4.1

An inverse relationship is observed between grafting density and the size of surfactant molecule. The smaller the surfactant, the higher grafting density is, and vice versa. For example, TGA is the smallest surfactant and the graft density is the highest. On the other hand, CTAB is the largest one; correspondingly, its density is the lowest. Based on this result, a compact packing of surfactant molecules on the surface of particles can be proposed for our system.

Surface charge is an important property of nanoparticles that determines the stability of dispersions. When a nanoparticle is dispersed in an aqueous solution, the ionization of surface groups and/or the adsorption of cations or anions result in the generation of a surface charge. Thus, an electric potential is developed between the particle surface and the dispersion medium. The electrostatic repulsion force between colloidal particles in the medium is featured by zeta potential measurements, which also can provide the isoelectric point (IEP). The IEP is defined as the pH at which the surface is neutrally charged. The surface charge is expected to change depending of the chemistry of surfactant. The effect of pH values on zeta potentials of both unmodified and modified CeO_2 nanoparticles is illustrated in Fig. 8.

The surface charge may vary from positive to negative as pH increases because of the deprotonation of the surface groups. For unmodified particles, the IEP is 4.4, which suggests that the surface of unmodified CeO_2 particles is negative. The surface of metal oxide nanoparticles dispersed in water is generally covered by hydroxyl groups [31]. Partial dissociation of hydroxyl groups can be the origin of negative surface charge. The usage of a positively charged surfactant, such as CTAB in our case, shows Coulombic interaction between the negative sites on the particles and shifts the IEP to higher pH (=9.9). On the other hand, the surface charge is not affected by the usage of silane surfactants, as seen when MPS is applied in our system. The grafting of MPS occurs mainly through surface hydroxyl groups and does not affect the charge balance on the particle surface. The IEP value is lower when TGA is used as a surfactant. Based on the results of vibrational spectroscopy discussed above, TGA molecules are grafted onto the particle surface mainly by condensation of —SH and surface —OH groups.

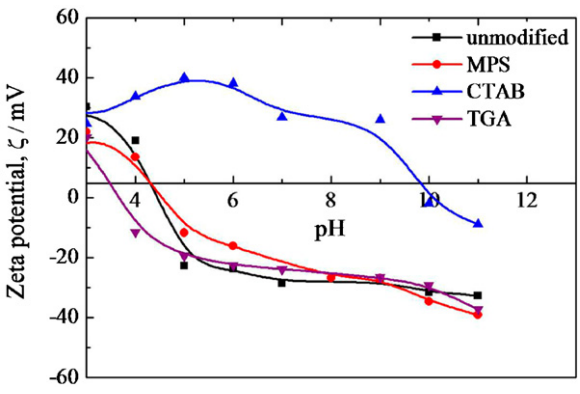

Fig. 8. Zeta potentials of unmodified CeO_2 particles and CeO_2 particles synthesized in the presence of MPS, CTAB, and TGA dependent on pH values.

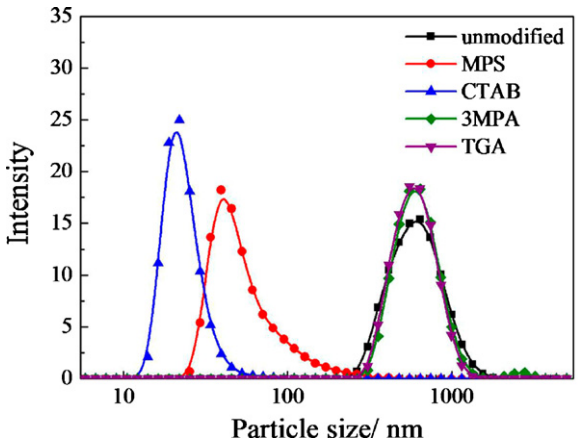

Fig. 9. Particle size distributions of the nanoparticles.

The carboxylic acid group of the surfactant molecule remains on the surface of particles. In an aqueous medium, it dissociates and forms carboxyl groups that make the surface even more negative (pH = 3.8). Accordingly, the surface charge can readily be controlled by the selection of the surfactant.

The surface-capped molecules prevent the nanoparticles aggregation and allow the CeO_2 nanocrystals to be redispersed in organic media. Particle size distributions of unmodified and surface-modified CeO_2 nanoparticles in methyl methacrylate (MMA) were investigated by DLS. The results are shown in Fig. 9.

MMA has a hydrophobic medium and the efficiency of the surface-modification process can be readily tested. The results suggest that the interactions between nanocrystals and organic media, that is, surface chemistry of particles, have a key role in the dispersion stability. The unmodified ceria particles exhibit a mean diameter of 0.6 μm (the size refers to aggregates of individual particles). 3-MPA and TGA modified particles showed comparable particle size distribution as in the unmodified ones. Both surfactants contain mercapto and carboxyl groups. Although the molecules are attached to the surface from mainly mercapto groups, both functional groups may coexist on the surface. As a result, the surface has some hydrophilic nature due to the presence carboxylic acid groups that reduces the compatibility with MMA. This result indicates that these surfactants are not a good choice to obtain homogeneous dispersions of particles in organic media. However, MPS- and CTAB-modified particles exhibited mean diameters of 40 nm and 20 nm, respectively, in the same monomeric medium. In MPS, the control of surfactant amount on the CeO_2 particles requires a systematic study. In our conditions, a high amount of SiO_2 network is formed due to the self-condensation of silane groups [32]. We can conclude that CTAB is the best surfactant from all aspects. Since the surface of CeO_2 nanoparticle has a negative potential, CTAB is attached to the surface from its cationic part via electrostatic forces. The long hydrophobic alkane group provides surface hydrophobicity and renders the size smallest among other surface modifiers.

3.3. Tentative mechanism of particle formation

At room temperature, the reaction of cerium(III) nitrate under basic conditions with ammonia results in the precipitation of gelatinous hydrous cerium(IV) oxide [7]. When ammonia is added to a cerium(III) precursor solution, immediate precipitation of $Ce(OH)_3$ is observed because of the low solubility constant of this compound ($K_{sp} = 7 \times 10^{-21}$) [13]. In an alkaline environment, $Ce(OH)_3$ is oxidized to hydrated Ce(IV) ions,[33] and then hydrolyzed to form the complex $[Ce(OH)_x(H_2O)_y]^{(4-x)+}$ [34,35]. Finally, the cerium(IV)

Table 3
Comparison of the intensity ratio of reflections (1 1 1) and (2 0 0) in XRD patterns.

CeO_2 nanocrystals	(1 1 1)/(2 0 0) intensity ratio	Morphology
CeO_2	2.95	Cuboctahedral
CeO_2-MPS	1.43	Cubic
CeO_2-CTAB	1.74	Cubic
CeO_2-3MPA	1.47	Cubic
CeO_2-TGA	1.49	Cubic

hydroxide complex is deprotonated by water molecules [33,36] and the nucleation of ceria nanoparticles occurs. The supersaturation degree of the initial precipitate and the oxidation of Ce(III) to Ce(IV) are strongly affected by the hydroxyl ion content in the process [13,36,].

The growth of CeO_2 nanocrystals can be examined by the correlation between the intensity of (1 1 1) and (2 0 0) crystallite planes in XRD patterns. The simple ratio between these most prominent planes can give some hints about the development of particle morphology. The result of our measurements for each particle is given in Table 3.

In the absence of surfactants, the growth of (1 1 1) planes dominates that of the (2 0 0) plane, that is, the (1 1 1) plane grows faster than the (2 0 0) one. Thus, the nanocrystals showed a cuboctahedral morphology. This ratio is reduced from 2.95 in the unmodified CeO_2 to approximately 1.50 in the surface-modified samples. In the presence of surfactant, the particles showed cubic morphology, regardless of the type of surfactants. The capping agents preferentially adsorb to (2 0 0) planes and suppress the growth of these planes. The relative growth of (1 1 1) planes exceeds the one of (2 0 0) ones. As a result, well defined cubic morphology is obtained.

4. Conclusion

In this study, controlled chemical precipitation of homogeneous CeO_2 nanoparticles of average size smaller than 10 nm with various surface functionalities was presented. The most significant aspect of our synthesis method is that almost any functionality can be introduced onto the surfaces of nanoparticles by choosing appropriate molecules as capping ligands. Although only thiol, aliphatic, and carboxylic groups are chosen here to demonstrate the idea, molecules with other functional groups such as aldehyde, epoxide, amine can also be used as the capping agents to build a specific ligand shell. The compatibility of the resulting particles with MMA demonstrated that the procedure can be developed into a general one for the preparation of ceria nanoparticles with versatile surface functionalities. This simple approach is promising for future large-scale synthesis of this nanostructured material for many important applications in catalysis, optoelectronics, and oxygen storage capacity medium in a controlled manner.

Acknowledgments

MMD acknowledges the financial support of the Scientific and Technological Research Council of Turkey (TUBITAK, project TBAG-109T905) and the Izmir Institute of Technology Material Research Center for XRD and TGA analysis. Dr. Ingo Lieberwith is thanked for the high-resolution TEM measurements. MMD thanks Prof. M. Çiftçioğlu for useful discussions.

References

[1] M. Taguchi, S. Takami, T. Naka, T. Adschiri, Growth mechanism and surface chemical characteristics of dicarboxylic acid-modified CeO_2 nanocrystals produced in supercritical water: tailor-made water-soluble CeO_2 nanocrystals, Cryst. Growth Des. 9 (2009) 5297–5303.
[2] A. Corma, P. Atienzar, H. García, J.Y. Chane-Ching, Hierarchically mesostructured doped CeO_2 with potential for solar-cell use, Nat. Mater. 3 (2004) 394–397.
[3] W.C. Maskell, Progress in the development of zirconia gas sensors, Solid State Ionics 134 (2000) 43–50.
[4] C. Larese, M.L. Granados, F.C. Galisteo, R. Mariscal, J.L.G. Fierro, TWC deactivation by lead: a study of the Rh/CeO_2 system, Appl. Catal. B: Environ. 62 (2006) 132–143.
[5] X.W. Lu, X.Z. Li, F. Chen, C.Y. Ni, Z.G. Chen, Hydrothermal synthesis of prism-like mesocrystal CeO_2, J. Alloys Compd. 476 (2009) 958–962.
[6] Z.C. Orel, B. Orel, Optical-properties of pure CeO_2 and mixed CeO_2/SnO_2 thin-film coatings, Phys. Status Solidi (b) 186 (1994) K33–K36.
[7] K.S. Lin, S. Chowdhury, Synthesis, Characterization, and application of 1-D cerium oxide nanomaterials: a review, Int. J. Mol. Sci. 11 (2010) 3226–3251.
[8] T. Masui, H. Hirai, R. Hamada, N. Imanaka, G. Adachi, T. Sakata, H. Mori, Synthesis and characterization of cerium oxide nanoparticles coated with turbostratic boron nitride, J. Mater. Chem. 13 (2003) 622–627.
[9] O. Kepenekci, M. Emirdag-Eanes, M.M Demir, Effect of alkali metal hydroxides on the morphological development and optical properties of ceria nanocubes under hydrothermal conditions, J. Nanosci. Nanotechnol. 11 (2011) 3565–3577.
[10] H. Oh, S. Kim, Synthesis of ceria nanoparticles by flame electrospray pyrolysis, J. Aerosol Sci. 38 (2007) 1185–1196.
[11] F. Zhang, S.W Chan, J.E. Spanier, E. Apak, Q. Jin, R.D. Robinson, I.P. Herman, Cerium oxide nanoparticles: size-selective formation and structure analysis, Appl. Phys. Lett. 80 (2002) 127–129.
[12] M. Palard, J. Balencie, A. Maguer, J.F. Hochepied, Effect of hydrothermal ripening on the photoluminescence properties of pure and doped cerium oxide nanoparticles, Mater. Chem. Phys. 120 (2010) 79–88.
[13] X.D. Zhou, W. Huebner, H.U. Anderson, Room-temperature homogeneous nucleation synthesis and thermal stability of nanometer single crystal CeO_2, Appl. Phys. Lett. 80 (2002) 3814–3816.
[14] M.M. Demir, D. Soyal, C. Unlu, M. Kus, S. Ozcelik, Controlling spontaneous emission of CdSe nanoparticles dispersed in electrospun fibers of polycarbonate urethane, J. Phys. Chem. C 113 (2009) 11273–11278.
[15] M.M. Demir, R. Muñoz-Espí, I. Lieberwirth, G. Wegner, Precipitation of monodisperse ZnO nanocrystals via acid-catalyzed esterification of zinc acetate, J. Mater. Chem. 16 (2006) 2940–2947.
[16] M.M. Demir, K. Koynov, U. Akbey, C. Bubeck, I. Park, I. Lieberwirth, G. Wegner, Optical properties of composites of PMMA and surface-modified zincite nanoparticles, Macromolecules 40 (2007) 1089–1100.
[17] R. Muñoz-Espí, Y. Qi, I. Lieberwirth, C.M. Gómez, G. Wegner, Surface-functionalized latex particles as controlling agents for the mineralization of zinc oxide in aqueous medium, Chem. Eur. J. 12 (2006) 118–129.
[18] T. Taniguchi, T. Watanabe, N. Sakamoto, N. Matsushita, M. Yoshimura, Aqueous route to size-controlled and doped organophilic ceria nanocrystals, Cryst. Growth Des. 8 (2008) 3725–3730.
[19] M. Taguchi, S. Takami, T. Adschiri, T. Nakane, K. Sato, T. Naka, Supercritical hydrothermal synthesis of hydrophilic polymer-modified water-dispersible CeO_2 nanoparticles, CrystEngComm 13 (2011) 2841–2848.
[20] S.H. Yu, H. Cölfen, A. Fischer, High quality CeO_2 nanocrystals stabilized by a double hydrophilic block copolymer, Colloids Surf. A 243 (2004) 49–52.
[21] K. Niesz, C. Reji, J.R. Neilson, R.C. Vargas, D.E. Morse, Unusual evolution of ceria nanocrystal morphologies promoted by a low-temperature vapor diffusion based process, Cryst. Growth Des. 10 (2010) 4485–4490.
[22] Z.L. Wang, X.D. Feng, Polyhedral shapes of CeO_2 nanoparticles, J. Phys. Chem. B 107 (2003) 13563–13566.
[23] U. Akbey, W.T. Franks, A. Linden, S. Lange, R.G. Griffin, B.J. van Rossum, H. Oschkinat, Dynamic nuclear polarization of deuterated proteins, Angew. Chem. Int. Ed. 49 (2010) 7803–7806.
[24] M. Lelli, D. Gajan, A. Lesage, M.A. Caporini, V. Vitzthum, P. Mieville, F. Heroguel, F. Rascon, A. Roussey, C. Thieuleux, M. Boualleg, L. Veyre, G. Bodenhausen, C. Coperet, L. Emsley, Fast characterization of functionalized silica materials by silicon-29 surface-enhanced NMR spectroscopy using dynamic nuclear polarization, J. Am. Chem. Soc. 133 (2011) 2104–2107.
[25] R.G. Griffin, Spectroscopy clear signals from surfaces, Nature 468 (2010) 381–382.
[26] O. Lafon, M. Rosay, F. Aussenac, X.Y. Lu, J. Trebosc, O. Cristini, C. Kinowski, N. Touati, H. Vezin, J.P. Amoureux, Beyond the silica surface by direct silicon-29 dynamic nuclear polarization, Angew. Chem. Int. Ed. 50 (2011) 8367–8370.
[27] A. Lesage, M. Lelli, D. Gajan, M.A. Caporini, V. Vitzthum, P. Mieville, J. Alauzun, A. Roussey, C. Thieuleux, A. Mehdi, G. Bodenhausen, C. Coperet, L. Emsley, Surface enhanced NMR spectroscopy by dynamic nuclear polarization, J. Am. Chem. Soc. 132 (2010) 15459–15461.
[28] S. Maensiri, C. Masingboon, P. Laokul, W. Jareonboon, V. Promarak, P.L. Anderson, S. Seraphin, Egg white synthesis and photoluminescence of platelike clusters of CeO_2 nanoparticles, Cryst. Growth Des. 7 (2007) 950–955.
[29] C.W. Sun, H. Li, H.R. Zhang, Z.X. Wang, L.Q. Chen, Controlled synthesis of CeO_2 nanorods by a solvothermal method, Nanotechnology 16 (2005) 1454–1463.
[30] M.G. Sujana, K.K. Chattopadyay, S. Anand, Characterization and optical properties of nano-ceria synthesized by surfactant-mediated precipitation technique in mixed solvent system, Appl. Surf. Sci. 254 (2008) 7405–7409.
[31] J.N. Israelachvili, Intermolecular and Surface Forces, Elsevier Netherlands, 2011.
[32] C.C. Chang, P.H. Chen, C.M. Chang, Preparation and characterization of acrylic polymer-nanogold nanocomposites from 3-mercaptopropyltrimethoxysilane encapsulated gold nanoparticles, J. Sol-Gel Sci. Technol. 47 (2008) 268–273.

[33] B. Djuricic, S. Pickering, Nanostructured cerium oxide: preparation and properties of weakly-agglomerated powders, J. Eur. Ceram. Soc. 19 (1999) 1925–1934.
[34] M. Hirano, E. Kato, Hydrothermal synthesis of nanocrystalline cerium(IV) oxide powders, J. Am. Ceram. Soc. 82 (1999) 786–788.
[35] P.L. Chen, I.W. Chen, Reactive cerium(IV) oxide powders by the homogeneous precipitation method, J. Am. Ceram. Soc. 76 (1993) 1577–1583.
[36] H.I. Chen, H.Y. Chang, Synthesis of nanocrystalline cerium oxide particles by the precipitation method, Ceram. Int. 31 (2005) 795–802.